RSC Advances

PAPER

View Article Online
View Journal | View Issue

Cite this: *RSC Adv.*, 2024, **14**, 19014

Graphitic carbon nitride supported silver nanoparticles (AgNPs/g-C_3N_4): synthesis and photocatalytic behavior in the degradation of 2,4-dichlorophenoxyacetic acid†

Phung Thi Lan, *[a] Nguyen Hoang Hao,[b] Nguyen Trung Hieu,[a] Nguyen Thi Thu Ha,[a] C. Trevor Brown[c] and Le Minh Cam[ad]

Graphitic carbon nitride supported silver nanoparticles (AgNPs/g-C_3N_4) with 1%, 3%, and 5% AgNPs were successfully synthesized by an "*ex situ*" method with ultrasound of a mixture of AgNP solution and g-C_3N_4. The AgNP solution was prepared by chemical reduction with trisodium citrate, and g-C_3N_4 was synthesized from the urea precursor. The supported nanoparticles were characterized by X-ray diffraction spectroscopy (XRD), scanning electron microscopy (SEM), transmission electron microscopy (TEM), nitrogen adsorption–desorption (BET), Fourier transformation infrared (FTIR) and Raman spectroscopy, ultraviolet-visible diffuse reflectance spectroscopy (UV-Vis DRS), photoluminescence spectroscopy (PL), electron paramagnetic resonance (EPR) and electrochemical impedance spectroscopy (EIS) Nyquist plots. The visible light-driven photocurrent measurement was performed by three on–off cycles of intermittent irradiation. The analyses show that AgNPs were evenly dispersed on g-C_3N_4, and have sizes ranging from 40 to 50 nm. The optical properties of the AgNPs/g-C_3N_4 material were significantly enhanced due to the plasmonic effect of AgNPs. The photocatalytic activity of catalysts was evaluated by 2,4-D degradation under visible light irradiation (λ > 420 nm). In the reaction conditions: pH 2.2; C_o (2,4-D) 40 ppm; a m/v ratio of 0.5 g L^{-1}, AgNPs/g-C_3N_4 materials exhibit superior photocatalytic activity compared to the pristine g-C_3N_4. The studies on the influence of free radicals and photogenerated holes, h^+, show that $^{\bullet}OH$, $O_2^{\bullet-}$, and h^+ play decisive roles in the photocatalytic activity of AgNPs/g-C_3N_4. The TOC result indicates the minimal toxicity of the by-products formed during the 2,4-D degradation. In addition, the AgNPs/g-C_3N_4 catalytic activity under direct sunlight irradiation was similar to that under artificial UV irradiation. Based on these results, a possible mechanism is proposed to explain the enhanced photocatalytic activity and stability of AgNPs/g-C_3N_4. Theoretical calculations on the interaction between 2,4-D and g-C_3N_4, Ag/g-C_3N_4 was also performed. The calculated results show that the adsorption of 2,4-D on Ag-modified g-C_3N_4 is significantly more effective compared to pristine g-C_3N_4.

Received 9th April 2024
Accepted 7th June 2024

DOI: 10.1039/d4ra02658f

rsc.li/rsc-advances

Introduction

Herbicides, especially chemicals that control undesired plants and protect crops, have played a crucial role in agriculture. However, excessive use and misuse of herbicides not only affects the quality of agricultural products, due to the proliferation of herbicide residues, but also directly contributes to environmental pollution in soil, water, and the atmosphere. 2,4-Dichlorophenoxyacetic acid (2,4-D) is a commonly used herbicide, and, if used excessively, can moderately persist, particularly in anaerobic environments, such as soil and water.[1] Bioaccumulation of 2,4-D can be highly toxic to aquatic life and has been associated with Parkinson's disease and autism in humans.[2] New methods to completely treat persistent organic chlorine compounds like 2,4-D are of great interest to the agriculture industry.

Currently, two main methods are used for 2,4-D treatment: adsorption[3–6] and advanced oxidation processes (AOPs) such as ozonation, Fenton oxidation, and photocatalysis.[7–10] Adsorption methods remove 2,4-D primarily from water. The 2,4-D is retained on the surface of adsorbent materials without degradation into environmentally friendly products. In contrast, AOPs have the potential to completely remove toxic chemicals

[a]*Faculty of Chemistry, Hanoi National University of Education, 136 Xuan Thuy, Cau Giay, Hanoi, Vietnam. E-mail: lanpt@hnue.edu.vn*
[b]*College of Education, Vinh University, 182 Le Duan, Vinh, Nghe An, Vietnam*
[c]*The UNE, Armidale, Australia*
[d]*Thanh Do University, QL 32, Kim Chung, Hoai Duc, Ha Noi, Vietnam*

† Electronic supplementary information (ESI) available. See DOI: https://doi.org/10.1039/d4ra02658f

from the environment. Photocatalysis is particularly attractive because it harnesses natural sunlight as an energy source.[7,11,12]

Graphite carbon nitride (g-C_3N_4), the metal-free semiconductor has been widely used in many applications such as chemical sensors, water splitting, and pollutant degradation[13–17] Graphitic carbon nitride (g-C_3N_4) is a promising material for the photocatalysis of 2,4-D.[12] It is synthesized from readily available, low-cost precursors (urea, melamine, thiourea, *etc.*), has high chemical and thermal stability, is not toxic, and has a moderate band gap energy of approximately 2.7 eV.[11] However, g-C_3N_4 has limitations, such as rapid electron–hole recombination rates and a small specific surface area. To enhance the catalytic activity of g-C_3N_4, it is combined with nano-sized metal semiconductor oxides like TiO_2,[18,19] WO_3,[20] or d-band metal nanoparticles like Ag, Au (AgNPs, AuNPs). Such additives cause plasmon effects, which enhance light absorption and thus photocatalytic activity.[21,22]

Nanoparticles (NPs) of noble metals (*i.e.*, Ag, Au, Pt) can strongly absorb visible light due to their surface plasmon resonance (SPR), which can be tuned by varying their size, shape and surrounding. Furthermore, noble metal NPs can also work as both electron traps and active reaction sites. These factors gave rise to a new approach to efficient visible-light photocatalysts. Recently, a variety of Ag-based semiconductor photocatalysts have been capturing considerable attention because of the surface plasmonic resonance (SPR) effect of noble metal nanoparticles under light irradiation. Han *et al.*[23] synthesized Ag@AgCl nanoframe photocatalyst. The as-synthesized samples showed superior photocatalytic activity and photo-generated charge carrier separation efficiency under visible light irradiation. Dong *et al.*[24] prepared uniform cubic Ag@AgCl photocatalysts and indicated that $O_2^{\bullet-}$ and Cl^0 are likely to be reactive species leading to the degradation of pollutants.

There have been few methods of Ag nano synthesis applied by research groups, for example Yao and co-authors[25] synthesized AgCl and then converted to Ag^0 by irradiation method (photolysis). The source of Cl^- ions to create AgCl is geothermal water. In the work of Zhou *et al.*[26] g-C_3N_4 was synthesized from calcining dicyandiamide in the N_2 stream. Ag/AgCl/gC_3N_4 was synthesized by a two-stage oxidation method. Zhang and co-authors[27] synthesized g-C_3N_4 from calcined melamine combined with hydrothermal then Ag@AgCl/g-C_3N_4 was synthesized by ion exchange method. In these synthesis methods the Ag contents were often not controlled resulting a quite high Ag content (10–40%) and therefore it could be the reason for low plasmon effect.

In this work, we aimed to enhance the photocatalytic performance of g-C_3N_4 for the photodegradation of 2,4-D by incorporating noble metal silver. The addition of Ag was intended to reduce electron–hole pair recombination and induce surface plasmon resonance, thereby boosting charge carrier generation. g-C_3N_4 was synthesized with varying amounts of Ag nanoparticles (3 wt%, and 5 wt% AgNPs/g-C_3N_4) using an "*ex situ*" ultrasound-assisted method. The structure, morphology, and optical properties of the synthesized samples were thoroughly investigated. The findings demonstrated that Ag nanoparticles were uniformly dispersed on the g-C_3N_4 surface, resulting in Ag/g-C_3N_4 photocatalysts with high photocatalytic activity and photochemical stability for 2,4-D degradation under visible light irradiation. The potential photocatalytic mechanism of charge transfer in Ag/g-C_3N_4 composites under visible light irradiation was explored in detail, considering energy levels and trapping experiments. This work offers a straightforward yet highly effective synthesis method for AgNPs/g-C_3N_4 and contributes to the development of novel visible light-driven photocatalysts.

Experimental

The main chemicals used in this research are from Sigma Aldrich with purity levels greater than 99.9%: urea, $(NH_2)_2CO$; trisodium citrate dihydrate, $Na_3C_6H_5O_7 \cdot 2H_2O$; silver nitrate, $AgNO_3$; citric acid hydrate, $C_6H_8O_7 \cdot H_2O$; sodium borohydride, $NaBH_4$; hydrochloric acid, HCl 37%; sodium hydroxide, NaOH. For 2,4-Dichlorophenoxyacetic acid $C_8H_6Cl_2O_3$ (2,4-D), its purity level is greater than 98%.

Synthesis of g-C_3N_4

Urea is finely ground and enclosed in aluminium foil, and then heated to 550 °C in a nitrogen atmosphere for 4 hours, with a heating rate of 5 °C min^{-1}. After heating, it is cooled to room temperature, washed three times with a 0.1 M nitric acid (HNO_3) solution, and then washed with distilled water until pH 7. Finally, the sample is dried at 80 °C for 12 hours, resulting in a pale-yellow powder.

Synthesis of AgNPs solution

AgNPs solutions are synthesized through reaction between silver nitrate and trisodium citrate at 60 °C, 70 °C, and 80 °C, and with reaction times of 45 minutes and 60 minutes. The synthesis process for the formation of stable AgNPs is optimized by varying $AgNO_3$ concentrations (0.1 M, 0.01 M, and 0.001 M) and trisodium citrate dihydrate ($Na_3C_6H_5O_7 \cdot 2H_2O$) concentrations (0.3 M and 0.03 M).

Synthesis of AgNPs/g-C_3N_4

The AgNPs/g-C_3N_4 catalyst is prepared by accurately weighing g-C_3N_4, and then sonicating with 100 mL of AgNPs solution for 1 hour at 20 °C. After sonication, the solution is allowed to settle, and the upper liquid portion is removed. Subsequently, the sample is dried at 40 °C for 12 hours, resulting in AgNPs/g-C_3N_4 material.

Three AgNPs/g-C_3N_4 catalysts with different weight percentages of AgNPs were synthesized. The mass of g-C_3N_4 was varied to produce 3 wt%, and 5 wt% AgNPs samples (1 wt% AgNPs was also prepared for comparison).

The crystalline phases of the synthesized catalyst samples were determined using X-ray diffraction (XRD) on a Bruker D8 Advance instrument (Germany) with a wavelength (λ) of 1.5406 Å. Light absorption capability and bandgap energies (E_g) of the samples were assessed using UV-visible diffuse reflectance spectroscopy (UV-Vis DRS) performed on a Shimadzu UV-2600 device. Surface morphology and the dispersion of AgNPs over g-

C_3N_4 were identified using scanning electron microscopy (SEM) performed on FESEM S-4800 equipment system and transmission electron microscopy (TEM) using JEM1010 device. Elemental compositions were determined through X-ray energy dispersive spectroscopy (EDX) using FESEM S-4800 equipment system. The textile properties of the samples were estimated from N_2 adsorption and desorption isotherms at 77 K using TriStar 3000 V6 07A equipment. Raman spectra were obtained using a Renishaw Raman system model 2000 spectrometer. Electron paramagnetic resonance (EPR) spectroscopy with center field of 3320 G, microwave frequency of 9.399 GHz and power of 0.05 mW was employed on Bruker EMX-Micro device to evaluate the presence of unpaired electrons.

The photoluminescence (PL) spectra of the photocatalysts were measured using FLS1000 Photoluminescence Spectrometer. The Fourier transform infrared (FTIR) spectra were recorded using FTIR spectrometer (model: Nicolet iS10, Thermo Scientific, USA).

The photocatalytic degradation reactions of 2,4-D over the synthesized catalyst samples were carried out in a photoreaction system. A quartz glass beaker is placed in a temperature-controlled bath at 25 °C, and a 250 W Xenon lamp is located 20 cm above the solution surface.

The experimental procedure was as follows: a specific volume (V mL) of the 2,4-D solution with an initial concentration of C_o (ppm), was mixed with a predetermined amount (m, mg) of AgNPs/g-C_3N_4. This mixture was stirred in the dark for 30 minutes, and then subjected to continuous illumination for a total of 210 minutes. At 30 minute intervals during irradiation, the 2,4-D concentration was monitored, using UV-visible absorption spectroscopy at a wavelength of 283 nm, to assess the catalytic activity of the synthesized samples. Additionally, the samples were analyzed using a TOC-VCSN analyzer (multi NC 2100S device) to quantify the residual total organic carbon content. To investigate the active species generated during the photocatalytic degradation process, capture experiments for free radicals (hydroxyl radicals ($^{\bullet}OH$), superoxide radicals ($O_2^{\bullet-}$), and holes (h^+)) were conducted using *tert*-butyl alcohol (*t*-BuOH), ascorbic acid (AA), and ethylenediaminetetraacetic acid disodium salt (EDTA-2Na), respectively.

Photoelectrochemical measurements were carried out using a precision potentiostat/galvanostat (model: AUTOLAB 302 N) with a standard three-electrode system, employing a Pt plate as the counter electrode and a saturated Ag/AgCl electrode as the reference electrode. A phosphate buffer solution (pH = 7) was used as the electrolyte. The working electrode, with an area of 1 cm^2, was prepared by coating FTO conductor glass with viscous pastes of pristine or Ag-doped graphitic carbon nitride using the doctor blade method and Scotch tape as a spacer. The pastes were prepared by mixing 30 mg of carbon nitride, 10 mg of ethyl cellulose, 10 mg of lauric acid, and 150 mg of terpineol. The coated films were subsequently dried overnight at 70 °C to improve their adhesion.

Electrochemical impedance spectra (EIS) were recorded over a frequency range of 0.1 Hz to 105 Hz. Photocurrent density measurements were performed within a potential range from −0.4 to 1.2 V *vs.* Ag/AgCl, with a potential scanning speed of 0.01 V s^{-1}.

Results and discussion

Optimization of the AgNPs synthesis process

Concentrations of $AgNO_3$ and $Na_3C_6H_5O_7$. Three $AgNO_3$ concentrations were investigated. For $C_{AgNO_3} = 0.1$ M mixed with 0.03 M and 0.3 M trisodium citrate, white precipitates immediately formed. These precipitates are silver citrate, trisodium citrate ($Ag_3C_6H_5O_7$). As the free Ag^+ ions are depleted, the reduction to form AgNPs cannot proceed.[28]

For $C_{AgNO_3} = 0.01$ M mixed with 0.03 M and 0.3 M trisodium citrate and then heated at 80 °C for 1 hour resulted in the precipitation of large free silver particles.

For $C_{AgNO_3} = 0.001$ M mixed with 0.3 M trisodium citrate and then heated at 80 °C for 1 hour resulted in free silver particles. Mixing with a 0.03 M trisodium citrate solution, however, resulted in a colloidal silver solution with an orange-silver hue, indicating the formation of AgNPs.

Reaction temperature. Three temperatures 60 °C, 70 °C, and 80 °C, were investigated. At 60 °C and 70 °C, the reaction rate is slow when 0.001 M $AgNO_3$ and 0.03 M trisodium citrate are mixed, and no AgNPs appeared after more than 1 hour. When the temperature is increased to 80 °C, a noticeable yellow colour change in the solution is observed within 20 minutes.

Reaction time. The extent of AgNPs formation when 0.001 M $AgNO_3$ was mixed with 0.03 M trisodium citrate, and heated at 80 °C was measured after 45 minutes and after 1 hour. After 45 minutes, 6.0 M HCl was added to the solution, and a white precipitate of AgCl was observed. This indicated that unreacted Ag^+ ions remain in the solution, and therefore incomplete reduction. After 1 hour, 6.0 M HCl was added, and there was no apparent white AgCl precipitate. The solubility product of AgCl $\approx 10^{-10}$, and so the Ag^+ concentration in the solution is very low, approximately 10^{-11} M. By 1 hour, Ag^+ ions had been completely reduced to Ag^0 nanoparticles.

From these findings, the process to synthesize AgNPs solutions is as follows: A mixture of 250 mL of 0.001 M $AgNO_3$ and 0.03 M trisodium citrate is heated at 80 °C and maintained for 1 hour in the absence of light. AgNPs form in accordance with the overall reaction:[29–31]

$$4Ag^+ + Na_3C_6H_5O_7 + 2H_2O \rightarrow 4Ag^0 + H_3C_6H_5O_7 + 3Na^+ + H^+ + O_2$$

The ratio of Ag^+ to $Na_3C_6H_5O_7$ is 1 : 4, and so the amount of citrate used is approximately 2.38 times the amount needed to completely reduce Ag^+. This excess citrate serves two purposes. The first is to ensure that the reaction proceeds to completion, with all Ag^+ ions reduced to free AgNPs, and the second is that citrate acts as a stabilizing agent for the AgNPs colloid system.[30]

UV-Vis absorption spectrum of AgNPs in solution. The characteristic UV-Vis absorption spectrum of AgNPs in solution is presented in Fig. S1,† covering the wavelength range from 300 to 700 nm.

The spectrum of the AgNPs solution reveals a maximum absorption peak at a wavelength (λ_{max}) of 441.7 nm, which falls within the visible light region. This result is entirely consistent with previous studies,[32–34] where nano Ag was successfully synthesized using a reduction method with trisodium citrate and β-D-glucose. Kamyar *et al.*[34] synthesized nano Ag using a reduction method with an extract from the turmeric plant. All studies[32–34] showed a UV-Vis maximum absorption peak of AgNPs in the wavelength range of 400–450 nm. The λ_{max} value shifts slightly within this wavelength range depending on reaction conditions such as the reducing agent used, the stabilizing agent for the AgNPs colloid system, reaction time, temperature, and Ag^+ concentration. Thus, in this work, by employing trisodium citrate as the reducing agent with a silver nitrate solution under the specified reaction conditions, AgNPs solutions were successfully synthesized.

Calibration curve for determining the concentration of the 2,4-D in solution. Eight standard solutions of 2,4-D with concentrations of 1, 2, 5, 10, 20, 40, 60, and 80 ppm at pH 2.2 were prepared and UV-vis scanned over the wavelength range, 190 nm to 500 nm. The spectra displayed two characteristic peaks at wavelengths, 229 and 283 nm. The absorption peak at 283 nm (Fig. S2a†) is attributed to the n → π* energy transition for the >C=O group in the 2,4-D molecule. During photodegradation of 2,4-D, intermediate products such as six-membered ring-containing compounds may appear and may absorb light at wavelengths smaller than 283 nm. Therefore, to ensure that the analysis of 2,4-D concentrations during photocatalysis is not affected by these intermediate products, a calibration curve at 283 nm is used for the quantification. The resultant 2,4-D calibration curve is shown in (Fig. S2b†). Linear regression of these data gives the following equation for the concentration of 2,4-D, $C_{2,4\text{-D}}$:

$$C_{2,4\text{-D}} = m_{Abs} - bC_{2,4\text{-D}}$$

where, m and b are constant, and Abs is absorption intensity.

Characteristics of AgNPs/g-C_3N_4

Elemental composition – EDX spectra. EDX spectra were measured for 3 wt% AgNPs/g-C_3N_4 and 5 wt% AgNPs/g-C_3N_4 to quantity the carbon, nitrogen, and silver content in the samples. The spectra are presented in Fig. S3† and elemental composition in Table 1.

Table 1 shows that there is a good agreement between the AgNPs content, measured from the EDX analyses (2.60 wt% and 4.00 wt%) and the stoichiometry of the synthesis mixtures. In addition, only three elements (C, N, and Ag) are clearly apparent in the spectra, and so the purity of each sample is high. The EDX result confirms that AgNPs successfully adsorbed the g-C_3N_4 surface. For convenience, the labels 3 wt% and 5 wt% AgNPs are used throughout this paper.

Table 1 Elemental composition (wt%) of two synthesized AgNPs/g-C_3N_4 samples

Samples	C	N	Ag	Total
3% AgNPs/g-C_3N_4	31.50	65.90	2.60	100.00
5% AgNPs/g-C_3N_4	29.81	66.20	4.00	100.00

Crystal structure of the AgNPs/g-C_3N_4 samples – XRD analysis. The XRD patterns g-C_3N_4, 3%AgNPs/g-C_3N_4 and 5%AgNPs/g-C_3N_4 are presented in Fig. 1.

Pure g-C_3N_4 and two AgNPs/g-C_3N_4 samples have a dominant peak at $2\theta = 27.4^\circ$ indexed to g-C_3N_4 (JCPDS 87-1526).[35] This peak is ascribed to the (002) plane of reflection in the g-C_3N_4 structure. In the XRD patterns of both 3 wt% AgNPs/g-C_3N_4 and 5 wt% AgNPs/g-C_3N_4 samples, four additional peaks appear at 2θ angles of 38.18°, 44.25°, 64.38°, and 77.27°, corresponding to the (111), (200), (220), and (311) planes, respectively, which are characteristic of the AgNPs crystal structure (JCPDS 87-717). These peaks have been previously reported.[33,34,36] These reflected planes indicate that AgNPs crystals have a face-centered cubic structure. Only Ag crystals exhibit plasmonic effects. No other crystalline impurities can be observed.

FT-IR analysis. The FT-IR spectra show similarities between the pristine g-C_3N_4 and AgNPs/g-C_3N_4 composites (Fig. 2). The peak at 1639.11 cm^{-1} can be attributed to the stretching vibration of C–N groups, while the group from about 1207.83 cm^{-1} to 1630 cm^{-1} can be attributed to the aromatic C–N stretching vibration. The peak at 813.94 cm^{-1} corresponds to the breathing mode of triazine units, and the peak at around 3283.44 cm^{-1} is attributed to the stretching vibration of the N–H group. These FT-IR peaks collectively indicate that the structure of g-C_3N_4 remains unchanged after loading with AgNPs.

Raman analysis. Raman spectroscopy is employed to provide insights into the chemical structures of g-C_3N_4 and AgNPs/g-C_3N_4. The Raman spectra of g-C_3N_4 and the composites exhibit several bands in the range of 700–1600 cm^{-1}, which are attributed to graphitic carbon nitride. In pristine g-C_3N_4, the G mode at around 1590 cm^{-1} arises from sp^2 C atoms, while the D mode at around 1340 cm^{-1} arises from sp^3 C atoms, indicating the formation of a graphitic-like structure.[37] In the case of

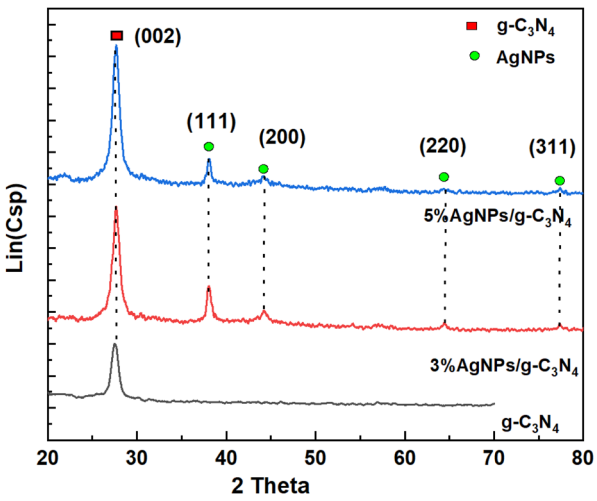

Fig. 1 XRD patterns of g-C_3N_4, 3 wt% AgNPs/g-C_3N_4 and 5 wt% AgNPs/g-C_3N_4.

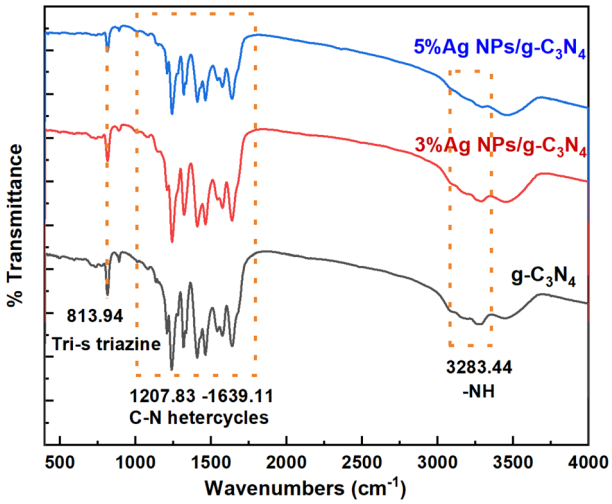

Fig. 2 FT-IR spectra of pristine g-C_3N_4 and AgNPs/g-C_3N_4 samples.

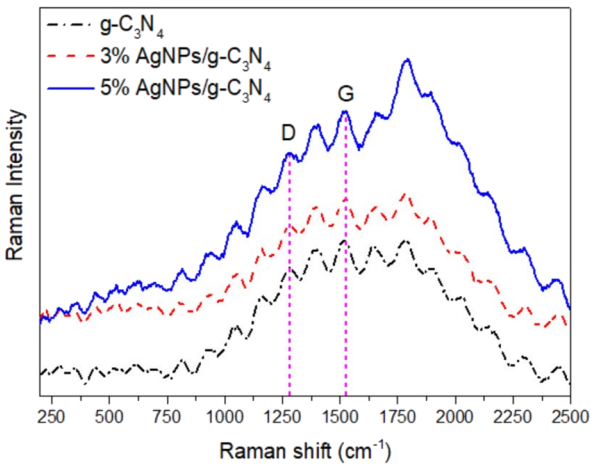

Fig. 3 Raman spectra of pure g-C_3N_4, and AgNPs/g-C_3N_4 composites.

AgNPs/g-C_3N_4 composites, both the characteristic peaks of g-C_3N_4 are clearly observed. The enhancement of Raman intensity could be attributed to the charge transfer between Ag and the g-C_3N_4 molecules (Fig. 3).[38]

BET surface area and porosity of the AgNPs/g-C_3N_4 samples. The BET surface area (S_{BET}) and porosity of g-C_3N_4, 3 wt% and 5 wt% AgNPs/g-C_3N_4, listed in Table 2 were calculated from N_2 adsorption–desorption isotherms at 77 K shown in Fig. 4. The

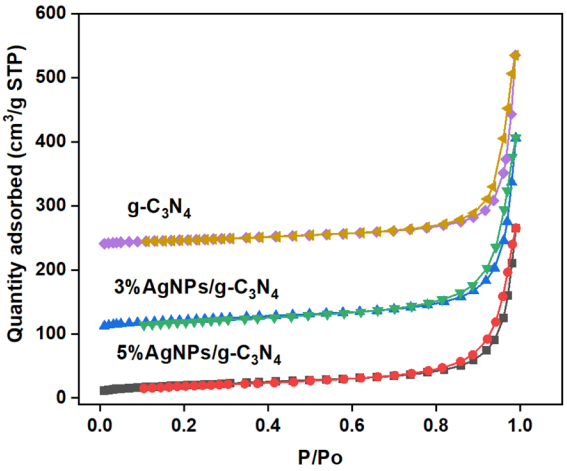

Fig. 4 Adsorption and desorption isotherms of N_2 at 77 K of g-C_3N_4, 3 wt% AgNPs/g-C_3N_4 and 5 wt% AgNPs/g-C_3N_4.

three samples demonstrate a typical type IV isotherm, characteristic of mesoporous materials. The BET surface area of g-C_3N_4 is 58 $m^2\ g^{-1}$ which increased to 69 $m^2\ g^{-1}$ and 78 $m^2\ g^{-1}$ after the introduction of 3 wt% and 5 wt% AgNPs, respectively. The average pore dimension (D) for g-C_3N_4 is 33.675 nm which decreased to 27.419 nm and 27.682 nm when AgNPs are present. The pristine g-C_3N_4 has a relatively low specific surface area, primarily consisting of an external surface (S_{ex}) and pore volume (V_{tot}) formed by voids between particles. AgNPs on the surface of g-C_3N_4 serve to increase the overall surface area (S_{BET}), particularly the external surface (S_{ex}), while the voids between g-C_3N_4 particles are filled.

The optical properties – UV-Vis DRS and PL spectra. Fig. 5a presents UV-Vis DRS spectra of g-C_3N_4, 3 wt% AgNPs/g-C_3N_4 and 5 wt% AgNPs/g-C_3N_4.

It is observed that pristine g-C_3N_4 can absorb visible light with an absorption edge at around 460 nm. The composites show a redshift in the absorption edge towards longer wavelengths. Compared to pristine g-C_3N_4, AgNPs/g-C_3N_4 composites exhibit an additional weak and broad peak around 450–750 nm, characteristic of the silver surface plasmon resonance band. Additionally, a much higher absorbance in the range of 500–800 nm is observed. These results indicate the positive influence of the plasmon effect generated by Ag NPs on the visible light absorption capability of AgNPs/g-C_3N_4 compared to pristine g-C_3N_4.

Energy bandgaps (E_g) are determined using the Kubelka–Munk equation:

Table 2 Surface area and porosity of the synthesized AgNPs/g-C_3N_4 samples[a]

Samples	S_{BET} ($m^2\ g^{-1}$)	S_{mi} ($m^2\ g^{-1}$)	S_{ex} ($m^2\ g^{-1}$)	V_{mi} ($cm^3\ g^{-1}$)	V_{ex} ($cm^3\ g^{-1}$)	V_{tot} ($cm^3\ g^{-1}$)	D (nm)
g-C_3N_4	58 ± 2	2 ± 0.5	56 ± 2	0.0012	0.4699	0.4711	33.675
3% AgNPs/g-C_3N_4	69 ± 2	9 ± 0.5	59 ± 2	0.0036	0.4049	0.4085	27.4619
5% AgNPs/g-C_3N_4	78 ± 5	10 ± 0.5	68 ± 3	0.0042	0.4683	0.4725	27.6820

[a] S_{BET} ($m^2\ g^{-1}$): BET surface area; S_{mi} ($m^2\ g^{-1}$): micropore surface area; S_{ex} ($m^2\ g^{-1}$): external surface area; V_{mi} ($cm^3\ g^{-1}$): micropore volume; V_{ex} ($cm^3\ g^{-1}$): external pore volume; V_{tot} ($cm^3\ g^{-1}$): total pore volume; D (nm): average pore dimension.

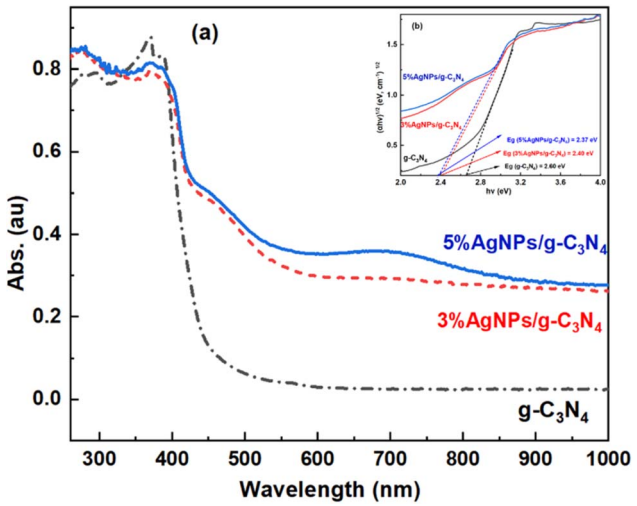

Fig. 5 UV-Vis DRS spectra of g-C_3N_4, 3 wt% AgNPs/g-C_3N_4 and 5 wt% AgNPs/g-C_3N_4 (a); plots of $(\alpha h\nu)^{1/2}$ against $h\nu$ for g-C_3N_4, 3 wt% AgNPs/g-C_3N_4 and 5 wt% AgNPs/g-C_3N_4 (b).

$$(\alpha h\nu)^n = A(h\nu - E_g)$$

where α is the optical absorption intensity (a.u.), h is the Planck's constant ($h = 6.625 \times 10^{-34}$ J s), ν is the frequency of the incident radiation ($\nu = c/\lambda$, where c is the speed of light and λ is the wavelength), $n = \frac{1}{2}$ and A is a proportionality constant.

Fig. 5b shows plots of $(\alpha h\nu)^{1/2}$ against $h\nu$, and from this, the band gap energy is the intersection of the tangent, dashed line with the $h\nu$ axis. The resultant E_g values of g-C_3N_4, 3% AgNPs/g-C_3N_4 and 5% AgNPs/g-C_3N_4 are 2.60 eV, 2.40 eV, and 2.37 eV, respectively. The E_g values of the AgNPs/g-C_3N_4 composites are significantly lower than those of pristine g-C_3N_4 which extends the absorption band into the visible light range. This phenomenon is likely to be a consequence of the plasmon effect on AgNPs. Remarkable absorption enhancement in visible light region is beneficial for improving photocatalytic behavior in this irradiation region.

Fig. 6 presents the PL spectra of pristine g-C_3N_4 and AgNPs/g-C_3N_4. Pristine g-C_3N_4 exhibits a strong emission peak at approximately 460 nm. Compared to pristine g-C_3N_4, the PL intensity of AgNPs/g-C_3N_4 composites decreases significantly. The weaker PL peak intensity indicates a slower recombination rate of photogenerated carriers, resulting in an increased availability of electrons and holes for the photocatalytic process of Ag/g-C_3N_4. However, excessive loading of Ag on g-C_3N_4, such as in the case of 5%-Ag/g-C_3N_4, causes the PL intensity to increase again, indicating a higher recombination rate of photogenerated carriers. It is evident that Ag/g-C_3N_4 composites with optimal amounts of Ag loading have the potential to serve as highly active photocatalysts. These findings strongly align with the results of the transient photocurrent density and EIS experiments.

EPR analysis. Electron paramagnetic resonance (EPR) was carried out to determine the formation of vacancy in synthesized samples. From Fig. 7, it can be seen that EPR of pristine g-C_3N_4 exhibits a symmetrical signal centered at $g = 2.018$, which relates to the unpaired electrons on sp^2 carbon in C–N heterocycle.[39] The stronger EPR signals from 3%AgNPs/g-C_3N_4 and 5% AgNPs/g-C_3N_4 in comparison to that of g-C_3N_4 due to the distribution of extra electrons to their nearest C atoms through the delocalized π-conjugated networks of g-C_3N_4. The strong EPR signal suggests a strong redox ability of photogenerated e^-/h^+ pairs from the composites upon light irradiation, and in this aspect the redox ability is highest with 3%AgNPs/g-C_3N_4 sample.

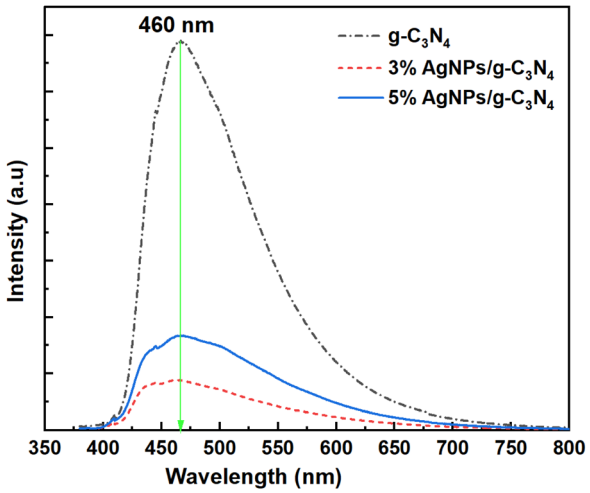

Fig. 6 PL spectra of the pristine g-C_3N_4 and AgNPs/g-C_3N_4 composites.

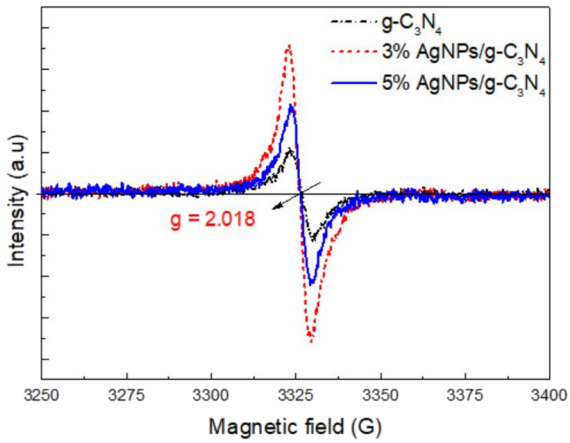

Fig. 7 Electron paramagnetic resonance (EPR) of pristine g-C_3N_4 and AgNPs/g-C_3N_4 composites.

Morphology and dispersion of AgNPs – SEM, EDX and TEM. The morphology of pristine g-C_3N_4 and of the composites, 3 wt% and 5 wt% AgNPs/g-C_3N_4 was analyzed by SEM and TEM. Fig. 8a presents the SEM images of these three samples. Pristine g-C_3N_4 presents soft agglomerate structure. AgNPs/g-C_3N_4 keeps the morphology of g-C_3N_4, and exhibits an exfoliated nanosheets texture. The elemental mappings of 3 wt% and 5 wt% AgNPs/g-C_3N_4 (Fig. 8b) indicate the successful loading and

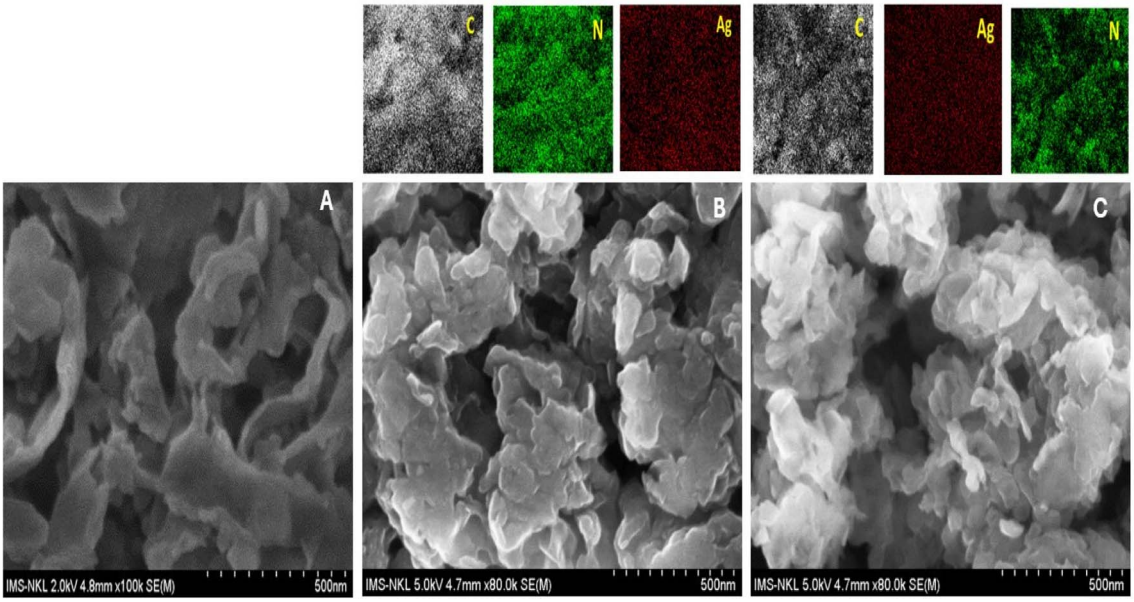

Fig. 8 SEM images and Energy dispersive X-ray (EDX) mapping analysis of carbon, nitrogen, silver and mixed for (A) g-C_3N_4, (B) 3% AgNPs/g-C_3N_4 and (b) 5% AgNPs/g-C_3N_4.

homogeneous dispersion of AgNPs throughout the surface of g-C_3N_4. The TEM image of g-C_3N_4 in Fig. 9 presents a sheet-like structure.

TEM images of 3 wt% and 5 wt% AgNPs/g-C_3N_4 show that AgNPs are observed as black dots with an average size of 40–50 nm and are uniformly dispersed on the surface of g-C_3N_4. These results are consistent with previous studies[32,34] that demonstrated the successful synthesis of AgNPs composites on g-C_3N_4.

Photocatalytic degradation of 2,4-D by AgNPs/g-C_3N_4

Illumination time. The photocatalytic degradation of 2,4-D is investigated over 1%, 3%, and 5% AgNPs/g-C_3N_4. For each experiment, 90 mg of the synthesized samples are mixed with 180 mL of 2,4-D solution ($C_o = 40$ ppm), and at a pH of 2.2. The mixture is left to achieve equilibrium adsorption in the dark for 30 minutes, and followed by photocatalysis for 240 minutes. The concentration of 2,4-D is monitored by UV adsorption throughout the photocatalysis by sampling at 30 minutes intervals. The UV-vis absorption spectra of the initial 2,4-D solution and of the solution after 180 minutes of illumination are presented in (Fig. S4†) for each of the three samples and g-C_3N_4.

The result shows that after 180 minutes of illumination, the characteristic absorption peak at 283 nm in the 2,4-D solution has completely disappeared, indicating that 2,4-D has decomposed into simpler compounds, including oxidation into CO_2 and H_2O. At 283 nm, the optical absorption values (A) for the mixtures with AgNPs/g-C_3N_4 are lower than the mixture with pure g-C_3N_4, and the lowest absorption is seen over the 3% AgNPs/g-C_3N_4.

The UV-Vis absorption spectra of the 2,4-D solution with 3% AgNPs/g-C_3N_4 at different illumination times were recorded (Fig. S5†).

After 60 minutes of illumination, optical absorption at 283 nm had decreased significantly and continued to decrease after 120, 150 and 180 minutes. After 180 minutes of illumination, the degradation of 2,4-D remained approximately constant, fluctuating around 94%. From the UV-Vis spectra, it is also

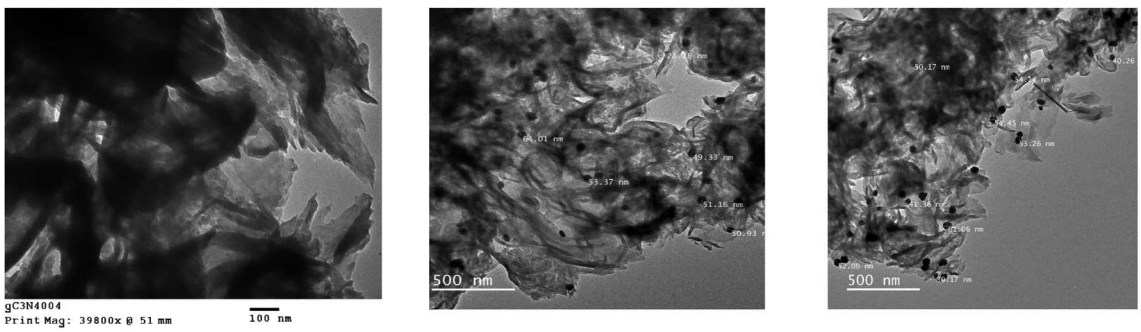

Fig. 9 TEM images of (a) g-C_3N_4 (b) 3% AgNPs/g-C_3N_4 and (c) 5% AgNPs/g-C_3N_4.

apparent that as 2,4-D decomposes, the A increases over the wavelength range of 240–260 nm. For the initial 2,4-D solution, the A values over this range are relatively low, but after 60 minutes of illumination, they increase. This indicates that 2,4-D has degraded into simpler organic structures that more strongly absorb radiation in the 240–260 nm range. As illumination time increases, the A values in this range gradually decrease and approach zero, suggesting that these intermediate products further decompose over time. To optimize the adsorption, and photocatalytic decomposition of 2,4-D, an illumination time of 210 minutes is chosen for the next analysis of the conditions.

Influence of AgNPs content. In this section, confirm the trend of the influence of Ag content, one more AgNPs/g-C_3N_4 sample (1%AgNPs/g-C_3N_4) was synthesized just for the purpose of comparing the activity with two samples 3% and 5%.

The variation of the 2,4-D concentration relative to the initial concentration C/C_o over illumination time t (min) is presented in Fig. 10.

The percentage efficiency, H% of treating 2,4-D is calculated from:

$$H\% = \left(1 - \frac{C}{C_o}\right) \times 100 \quad (1)$$

The experimental results show that the materials weakly adsorb 2,4-D. In the first 50 minutes of illumination, the decrease in 2,4-D concentration is not significant, and H% increases at most by 10–15% for all samples. This indicates that 2,4-D only weakly adsorbs to the samples and is consistent with an induction period for the photocatalytic reaction to commence. Time is initially required to form free radicals, $O_2^{\bullet-}$, $^{\bullet}OH$, and photo-induced electrons and holes. After 90 minutes of illumination (at the 120 minute mark in Fig. 10), the H% of 2,4-D over the samples starts to become significant. The 2,4-D degradation efficiency over g-C_3N_4 and 1% AgNPs/g-C_3N_4 is equivalent, at 32.6%. The 3% and 5% AgNPs/g-C_3N_4 samples exhibit better performance, reaching 41.7% and 36.8% efficiencies, respectively. After 120 minutes of illumination (at the 150 minutes mark in Fig. 10), the efficiency differences become more pronounced, with H% values following the sequence: g-C_3N_4 < 1% AgNPs/g-C_3N_4 < 5% AgNPs/g-C_3N_4 < 3% AgNPs/g-C_3N_4 (at 47.9%, 57.9%, 61.6%, and 73.6%, respectively). After 150 minutes of illumination, the 2,4-D degradation efficiency over g-C_3N_4 reaches 79.97%, while over % AgNPs/g-C_3N_4 an efficiency of 91.0% is achieved. After 210 minutes of illumination, when the concentrations of 2,4-D in the solutions are very low, and the differences in degradation efficiencies between the samples are less significant. However, the 3% AgNPs/g-C_3N_4 sample still exhibits the largest H% value at 92.4%. Therefore, it can be concluded that the photocatalytic activity of the samples increases in the order of g-C_3N_4 < 1% AgNPs/g-C_3N_4 < 5% AgNPs/g-C_3N_4 < 3% AgNPs/g-C_3N_4. The superior 2,4-D degradation efficiencies of AgNPs/g-C_3N_4 when compared to pure g-C_3N_4, reflect the role of AgNPs, and are consistent with published findings. Kashyap *et al.*[36] proposed a photocatalytic mechanism for 2,4-D decomposition over g-C_3N_4 supported by Ag NPs and Au NPs and explained that Ag NPs facilitate electron transfer between the conduction band of g-C_3N_4 and the reaction agents through surface plasmon resonance (SPR). This causes a reduction in the rate of recombination of photogenerated electrons and holes. Also, Ag NPs exhibit strong absorption in the visible light range, narrowing the bandgap of the g-C_3N_4 material, allowing it to be more active in the visible light spectrum.

Fig. 11 showed the dependence of $\ln(C_o/C)$ *vs.* time (t) over synthesized materials.

As shown in Fig. 11, the photodegradation of 2,4-D followed a first-order kinetic model over the 3% AgNPs/g-C_3N_4 composites under the experimental conditions established. From the linear form of $\ln(C_o/C)$ *vs.* time (t), the rate constants were calculated. The kinetic parameters of the photocatalytic degradation of 2,4-D are presented in Table 3.

Reusability studies. Furthermore, the photocatalytic stability of AgNP/g-C_3N_4 was evaluated through a 5-run cycling test under the same conditions. As shown in Fig. 12, 2,4-D is rapidly degraded after each 2,4-D decomposition experiment. No significant reduction in the photocatalytic activity of AgNPs/g-C_3N_4 was observed over five consecutive trials. Combined with the characterizations of the used AgNPs/g-C_3N_4, the results indicate that the AgNPs/g-C_3N_4 composites can serve as effective and stable photocatalysts for 2,4-D degradation.

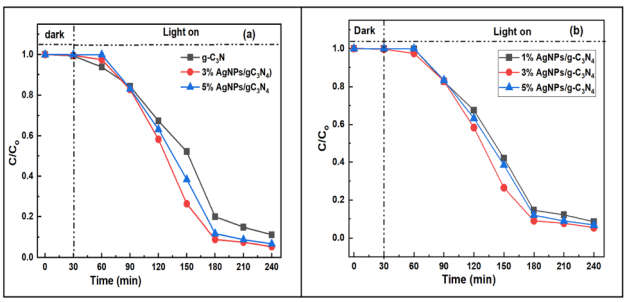

Fig. 10 Relative concentrations of 2,4-D as a function of illumination time in g-C_3N_4 and in 3% and 5% AgNPs/g-C_3N_4. Illumination commenced at 30 minutes.

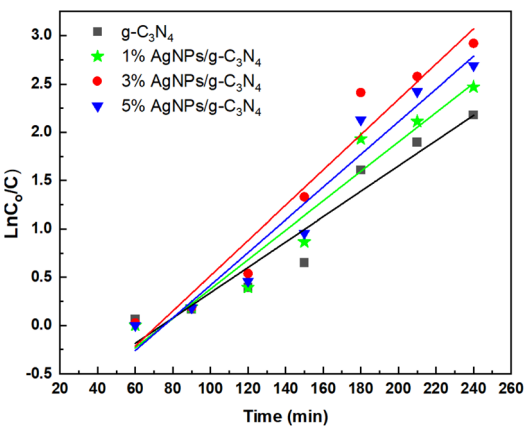

Fig. 11 The dependence of $\ln(C_o/C)$ *vs.* time (t) for photocatalytic degradation of 2,4-D over synthesized materials.

Table 3 Kinetic parameters of 2,4-D photocatalytic degradation of 2,4-D over synthesized materials[a]

Materials	g-C_3N_4	1%AgNPs/g-C_3N_4	3%AgNPs/g-C_3N_4	5%AgNPs/g-C_3N_4
k_{ap} (min^{-1})	0.0131	0.0152	0.0182	0.0169
R^2	0.9380	0.9463	0.9522	0.9459

[a] The findings showed that the photocatalytic rate constant changes slightly when g-C_3N_4 is coupled with AgNPs, increasing in the following order: g-C_3N_4 < 1%AgNPs/g-C_3N_4 < 5% AgNPs/g-C_3N_4 < 3% AgPNs/g-C_3N_4.

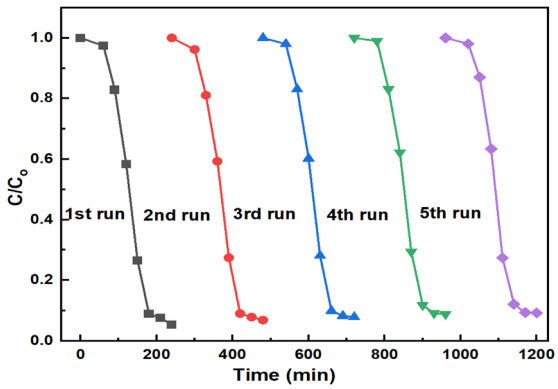

Fig. 12 Stability study for the photocatalytic 2,4-D degradation by 3% AgNP/g-C_3N_4 under visible light illumination.

On the other hand, after the reuse cycles, an XRD study was conducted (Fig. 13) to determine if there were any changes in the material. However, no significant changes were found in the structure of the catalyst.

As 3% AgNPs/g-C_3N_4 is the most efficient material for 2,4-D degradation, it was used to investigate other factors in the degradation process.

Influence of 2,4-D initial concentration. Three experiments were conducted concurrently using 20 mg of 3% AgNPs/g-C_3N_4, 40 mL of 2,4-D solution with concentrations of 20, 40, and 60 ppm, and a pH of 2.2. The mixtures were stirred in the dark for 30 minutes, followed by 210 minutes of illumination. The concentrations of 2,4-D are measured after 30 minutes in the dark and after 210 minutes of illumination. The results are shown in Fig. 14A.

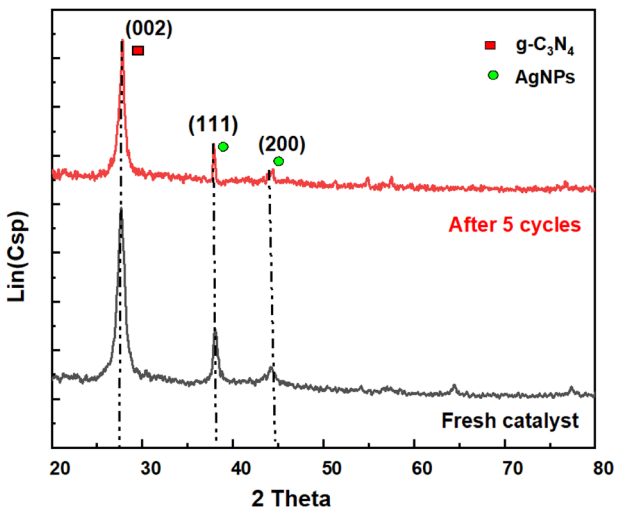

Fig. 13 XRD of 3% AgNPs/g-C_3N_4 before and after cycles of 2,4-D photodegradation.

At the lower initial concentrations of 2,4-D (20 ppm and 40 ppm), the treatment efficiency is high, reaching 93.5%, and 92.4%, respectively. However, at the highest initial concentration (60 ppm), the degradation efficiency dropped significantly to 70.50%. This decrease in treatment efficiency as the pollutant concentration increases is consistent with previous studies.[40,41] In the subsequent experiments, an initial 2,4-D concentration of 40 ppm is used.

Influence of pH. Three parallel experiments were conducted with three 2,4-D solutions with a concentration of 40 ppm, and a pH: 2.2, 5.5, or 8.2. In each solution, 20 mg of 3% AgNPs/g-C_3N_4 is added. The solutions were stirred in the dark for 30 minutes, followed by 210 minutes of illumination. The degradation efficiency results are presented in Fig. 14B.

The degradation efficiency of 2,4-D with 3% AgNPs/g-C_3N_4 decreases significantly as the pH of the solution increases. The higher the pH value, the lower the 2,4-D treatment efficiency. Efficiency decreases from 93.5% to 78.2% to 58.2% when the pH increases from 2.2 to 5.5 to 8.2. This result is consistent with previous publications[18] and can be explained by:

(1) At pH below 4.88, the following chain reactions are initiated that produce more $O_2^{\cdot -}$ and $^{\cdot}OH$ free radicals:[18]

$$O_2^{\cdot -} + H^+ \leftrightarrow HO_2^{\cdot}\ pK_a = 4.88$$

$$HO_2^{\cdot} \rightarrow O_2 + H_2O_2$$

$$HO_2^{\cdot} \rightarrow O^{2\cdot -} + HO_2^- + O_2$$

$$HO_2^- + H^+ \rightarrow H_2O_2$$

$$H_2O_2 + e^- \rightarrow {}^{\cdot}H_2O_2$$

$${}^{\cdot}H_2O_2 + O^{2\cdot -} \rightarrow {}^{\cdot}OH + OH^- + O_2$$

$$H_2O_2 \rightarrow 2{}^{\cdot}OH$$

(2) As pH increases, a portion of 2,4-D exist in the form of salt anions, which may affect its ability to participate in the photocatalytic reaction:

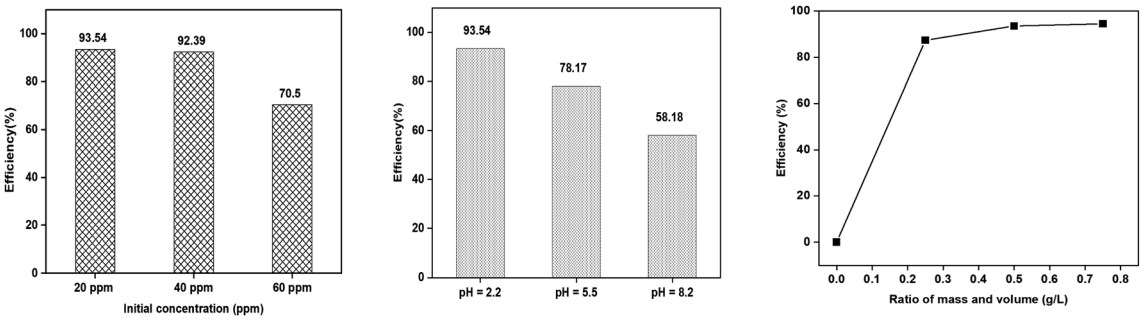

Fig. 14 (A) The efficiency, *H%* of 2,4-D treatment as a function of initial concentration, C_o (pH = 2.2; 210 minutes illumination). (B) The efficiency of 2,4-D treatment with 3% AgNPs/g-C_3N_4 at different pH (C_o = 40 ppm; 210 min illumination). (C) The influence of m/v ratio on the 2,4-D treatment (C_o = 40 ppm, pH = 2.2 and 3% AgNPs/g-C_3N_4).

$$C_8H_6Cl_2O_3 + OH^- \rightarrow C_8H_5Cl_2O_3^- + H_2O$$

Therefore, a pH of 2.2 is chosen to maximize the photocatalytic activity of 2,4-D.

Influence of the catalyst mass to solution volume ratios (g L^{-1}). Three parallel experiments were conducted with catalyst mass to solution volume ratios (g L^{-1}) of 0.25, 0.50, and 0.75. An amount of 10 mg, 20 mg, and 30 mg of 3% AgNPs/g-C_3N_4 were added to the same volume (40 mL) of a 40 ppm 2,4-D solution at pH 2.2. The mixtures were stirred in the dark for 30 minutes and then exposed to light for 210 minutes. The 2,4-D concentrations were measured after 30 minutes of stirring in the dark and after 210 minutes of exposure to light. The degradation efficiency results are presented in Fig. 14C.

From Fig. 14C, at mass-to-volume ratios of 0.75 g L^{-1}, 0.5 g L^{-1}, and 0.25 g L^{-1}, the degradation efficiency of 2,4-D is 94.5%, 92.4%, and 87.3%, respectively. Larger catalyst masses provide more surface area for the absorption of radiation, resulting in more photogenerated electron–hole pairs and free radicals. As a consequence, 2,4-D degradation improves. For this study, a ratio of 0.50 g L^{-1} is chosen, because, at higher ratios, the degradation efficiency did not differ significantly, and so conserved catalyst material and energy.

Mineralization of 2,4-D. The potential viability of the AgNPs/g-C_3N_4 photocatalyst is assessed through the mineralization efficiency of the 2,4-D. TOC during the photocatalytic reactions was recorded to investigate the mineralization of 2,4-D. The result is shown in Fig. 15. After 240 min irradiation about 80.2% TOC are removed, indicating that 2,4-D has not only been degradation but also efficiently mineralized over AgNPs/g-C_3N_4 under visible light irradiation.

The photoelectrochemical properties of pristine g-C_3N_4 and AgNPs/g-C_3N_4. To further study the efficiency of synthesized samples on the separation of electron–hole pairs the transient photocurrent density and electrochemical impedance spectroscopy (EIS) experiments were curried out.

The transient photocurrent responses *via* three on–off cycles of g-C_3N_4 and AgNPs/g-C_3N_4 under visible light illumination are shown in Fig. 16. The photocurrent intensity of g-C_3N_4 increases after introducing Ag, indicating Ag plays an important role in electronic transmission. As revealed by the PL analysis, the result confirms that there is a lower rate of recombination of photogenerated electron–hole pairs on AgNPs/g-C_3N_4 compared to that on pristine g-C_3N_4. Under light irradiation, the generated photocurrent of 3%AgNPs/g-C_3N_4 electrode is highest, thus 3% AgNPs/g-C_3N_4 holds strongest visible light irradiation, which is well in agreement with photocatalytic activities.

The Nyquist plots with pristine g-C_3N_4, and 3% (5%) AgNPs/g-C_3N_4 as photoanodes under visible light illumination are shown in Fig. 16. In general, a smaller arc radius in an EIS Nyquist plot corresponds to an effective separation and faster transfer of charges at the semiconductor/electrolyte interface.[42] The arc radii of AgNPs/g-C_3N_4 composites were smaller than that of pristine g-C_3N_4, signifying AgNPs/g-C_3N_4 composites have the higher efficiency in charge separation and electron transfer. The photoelectrochemical results confirm that the addition of Ag considerably improves the electro–hole pairs transfer and enhances the photocatalytic activity.

Possible pathway for photodegradation of 2,4-D over AgNPs/g-C_3N_4

Radical trapping experiments. Three free radicals $O_2^{\bullet-}$, $^{\bullet}OH$, and photogenerated holes were investigated to reveal the

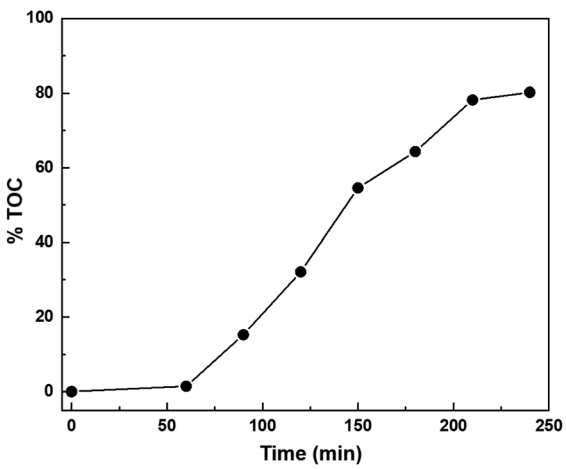

Fig. 15 TOC measurement during 2,4-D degradation process on 3% AgNPs/g-C_3N_4.

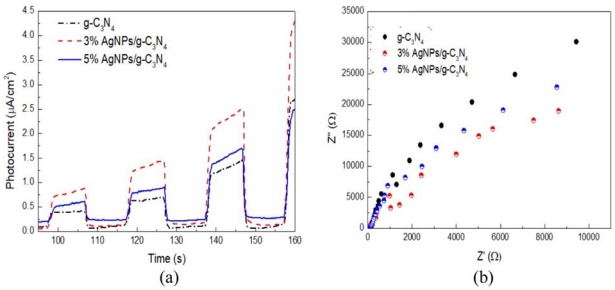

Fig. 16 (a) Transient photocurrents, (b) EIS Nyquist plots under visible light irradiation.

contribution of these radicals to the 2,4-D degradation in the reaction. The radical scavengers used are ascorbic acid-AA (for $O_2^{\bullet-}$), isopropyl alcohol (IPA) (for $^{\bullet}OH$), and Na-EDTA (for photogenerated h^+ holes). Each experiment used 80 mg of 3% AgNPs/g-C_3N_4 in 160 mL of a 40 ppm 2,4-D solution at pH 2.2. The mixtures are stirred in the dark for 30 minutes. Then, 16 mL of pure isopropyl alcohol radical scavenger is added to one of the solutions, and the mixture is exposed to light. After illumination times of 60, 90, 120, 150, and 180 minutes, the remaining 2,4-D concentration in the solution is determined. The same procedure is repeated with 16 mL of 0.1 M Na-EDTA, and 16 mL of 0.01 M ascorbic acid as radical scavengers. The results are presented in Fig. 17.

From Fig. 17, the degradation efficiency of 2,4-D with 3% AgNPs/g-C_3N_4 significantly decreased when introducing the radical scavengers AA, IPA and Na-EDTA into the reaction system. When no radical scavengers are added, the 2,4-D removal efficiency reached 92.4%, which is 1.83 times higher compared to when radical scavengers are present, indicating that $O_2^{\bullet-}$, $^{\bullet}OH$ and photogenerated h^+ holes are integral to the decomposition of 2,4-D. During the irradiation period from 60 to 180 minutes, AA display an inhibiting effect much stronger than IPA and Na-EDTA, suggesting that the $O_2^{\bullet-}$ has a more pronounced effect than $^{\bullet}OH$ radical and h^+ holes in the degradation of 2,4-D. Our result is in agreement with Kashyap *et al.*,[36] who have proposed a mechanism for the photocatalytic oxidation and decomposition of 2,4-D over Ag/g-C_3N_4. This mechanism includes the direct participation of $O_2^{\bullet-}$, $^{\bullet}OH$ radicals, and photogenerated h^+ holes.

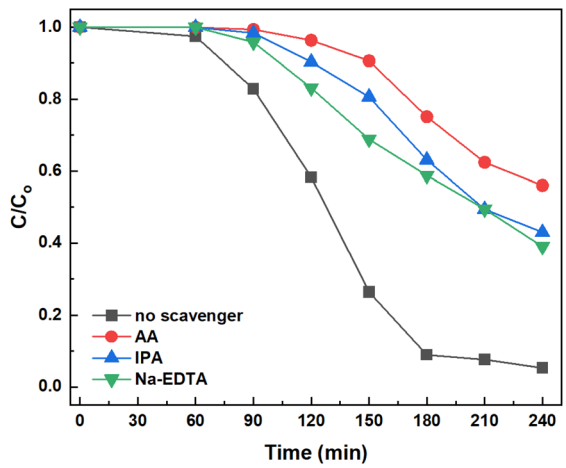

Fig. 17 The influence of $O_2^{\bullet-}$, $^{\bullet}OH$ radicals and photogenerated holes h^+ on the 2,4-D treatment (C_o = 40 ppm, pH = 2.2, 3% AgNPs/g-C_3N_4, 16 mL of 0.1 M Na-EDTA, 16 mL of isopropyl alcohol (IPA) and 1 mL of AA).

A possible mechanism discussion. A mechanism for the charge separation and transport of the electron–hole pairs over AgNPs/g-C_3N_4 under visible light illumination was proposed, based on the results of this study. The transfer of photoexcited e^- and h^+ depends on the relative band edge positions of the valence band (VB) and conduction band (CB) potentials, and E_g. In our work, the CB and VB potentials of the samples are estimated using eqn (2) and (3) (ref. 43–45)

$$E_{VB} = \chi - E^e + 0.5E_g \quad (2)$$

$$E_{CB} = E_{VB} - E_g \quad (3)$$

where χ is the electronegativity (~4.73 eV for g-C_3N_4); E^e is the energy of free electrons on the hydrogen scale (~4.5 eV); E_g is the energy band gap. The estimated VB and CB potentials for g-C_3N_4 are 1.53 eV and −1.07 eV, respectively.

When stimulated with a suitable light source the electrons are excited from VB to CB on g-C_3N_4, resulting in a CB rich in electrons (e^-) and leaving behind in the VB holes (h^+). The accumulated electrons on g-C_3N_4 migrate to the surface of Ag because the Fermi level of g-C_3N_4 is lower than that of Ag.[46] These photoelectrons react with water-dissolved oxygen (the reduction potential of oxygen −0.046 eV *vs.* NHE) to generate superoxide radicals ($O_2^{\bullet-}$). On the other hand, the potential for the $^{\bullet}OH/H_2O$ (2.68 eV *vs.* NHE) is too positive for the holes (h^+) in the VB of g-C_3N_4 to react with water to produce $^{\bullet}OH$ radicals. However, the scavenger experiments confirmed the existence of $^{\bullet}OH$ implying that $^{\bullet}OH$ should be produced through the multiple-electron reduction reaction of $^{\bullet}O_2^-$ conversion.[47] Finally, based on the result of trap experiments the VB h^+ of g-C_3N_4 would directly react the 2,4-D.

In this work, all the experiments were conducted at pH value of 2.1 then the effect of pH value could be described as eqn (4)–(11):[45,48,49]

$$g\text{-}C_3N_4 + h\nu \rightarrow g\text{-}C_3N_4\ (e^- + h^+) \quad (4)$$

$$g\text{-}C_3N_4\ (e^-) \rightarrow Ag\ (e^-) \quad (5)$$

$$Ag\ (e^-) + O_2 \rightarrow {}^{\bullet}O_2^- \quad (6)$$

$$^{\bullet}O_2^- + H^+ \rightarrow HO_2^{\bullet} \quad (7)$$

$$2HO_2^{\bullet} \rightarrow H_2O_2 + O_2 \quad (8)$$

$$H_2O_2 + e^- \rightarrow {}^{\bullet}OH + HO^- \quad (9)$$

$$H_2O_2 + h\nu \rightarrow 2{}^{\bullet}OH \quad (10)$$

$$2,4\text{-D} + {}^{\bullet}O_2^{-}/{}^{\bullet}OH/h^{+} \rightarrow \text{products} \quad (11)$$

The photocatalytic activity under direct sunlight. Considering the potential use of AgNPs/g-C_3N_4 as a photocatalyst in a wastewater treatment, the 3% AgNPs/g-C_3N_4 catalytic activity was evaluated on 2,4-D degradation under direct sunlight irradiation. The results are presented in Fig. 18. It can be seen the 3% AgNPs/g-C_3N_4 catalytic activity was similar under UV and direct sunlight irradiation, indicating that AgNPs/g-C_3N_4 is a promising catalyst to be used in a wastewater treatment with natural irradiation source. Inset also present.

Theoretical calculations on the interaction between 2,4-D and g-C_3N_4, Ag/g-C_3N_4. The theoretical simulation is also conducted to confirm a good interaction between 2,4-D and studied photocatalysts. The g-C_3N_4 model employed in theoretical calculations is the corrugated g-C_3N_4 model as described in ref. 50 and 51. All optimization and energy calculations were performed using the GFN2-xTB method, an accurate and broadly parameterized self-consistent tight-binding quantum chemical method incorporating multipole electrostatics and density-dependent dispersion contributions[52] This method has demonstrated high efficiency and effectiveness for calculations involving large systems.

The optimized adsorption configurations of 2,4-D on g-C_3N_4 and Ag/g-C_3N_4 are presented in Fig. S6 and S7,† respectively. Table S1† summarizes the calculated results for the adsorption processes. The adsorption of 2,4-D on Ag-modified g-C_3N_4 is significantly more effective compared to pristine g-C_3N_4. This is evident from various adsorption parameters such as adsorption energy, the shortest distance (d_{min}) from 2,4-D to g-C_3N_4, the charge transfer, and the bond order (BO) formed between 2,4-D and g-C_3N_4, as presented in Table S1.† The adsorption energy of 2,4-D on Ag/g-C_3N_4 is −271.3 kJ mol^{-1}, which is substantially more negative than the adsorption energy of 2,4-D on pristine g-C_3N_4, which is −95.9 kJ mol^{-1}. The d_{min} distance from 2,4-D to pristine g-C_3N_4 is 3.098 Å, significantly larger than the sum of the covalent radii of C and Cl (0.730 + 1.020 = 1.750 Å) or N and Cl (0.710 + 1.020 = 1.730 Å). In contrast, the d_{min} distance from 2,4-D to Ag-modified g-C_3N_4 is 2.254 Å, approximately equal to the sum of the covalent radii of Ag and O (1.450 + 0.660 = 2.110 Å).[53] There is a charge transfer (q) from Ag/g-C_3N_4 to 2,4-D (0.243 e), and the bond order (BO) formed between 2,4-D and Ag atoms is 0.780. This indicates that the adsorption of 2,4-D on Ag-modified g-C_3N_4 is a chemisorption process, involving the formation of covalent bonds between atoms in 2,4-D and the Ag atoms. In contrast, the adsorption process of 2,4-D on pristine g-C_3N_4 is physical adsorption, dominated by van der Waals interactions.

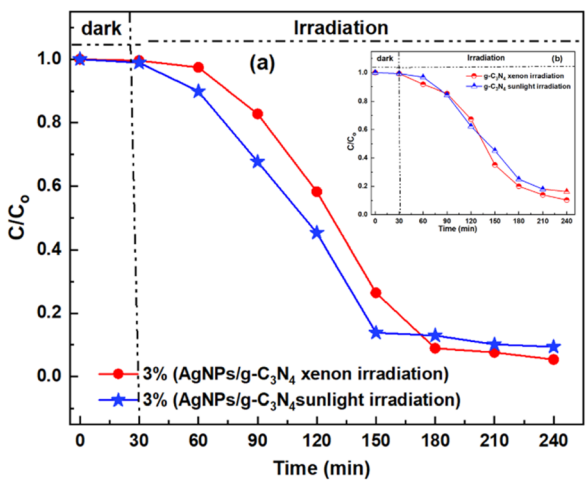

Fig. 18 2,4-D photodegradation over 3% AgNPs/g-C_3N_4 and g-C_3N_4 under UV irradiation and direct sunlight irradiation.

Conclusions

Three samples of AgNPs/g-C_3N_4 were successfully synthesized with AgNPs content of 3%, and 5% using an "*ex situ*" method with the assistance of ultrasound from AgNPs solutions and g-C_3N_4. The AgNPs solutions were synthesized using a citrate-assisted reduction method, and g-C_3N_4 was synthesized from a urea precursor. The characterization of the samples was carried using X-ray diffraction spectroscopy (XRD), scanning electron microscope (SEM), transmission electron microscopy (TEM), Nitrogen adsorption–desorption (BET), Fourier transformation infrared spectroscopy (FTIR), ultraviolet-visible diffuse reflectance spectroscopy (UV-Vis DRS) and photoluminescence spectroscopy, electron paramagnetic resonance (EPR). The visible-light-driven photocurrent measurement was performed by three on–off cycles of intermittent irradiation. The AgNPs were evenly distributed on g-C_3N_4 and have relatively small nanoscale sizes ranging from 40 to 50 nm. It was revealed that the plasmonic effect of AgNPs played an important role in broadened visible-light absorption and efficient electron–hole separation, mainly accounting for the improved photocatalytic activity. The investigation on the influence of ${}^{\bullet}OH$, $O_2^{\bullet-}$ radicals and photogenerated holes (h^+) demonstrating that h^+, ${}^{\bullet}OH$, and $O_2^{\bullet-}$ play crucial roles in the photocatalytic activity of the AgNPs/g-C_3N_4 catalysts.

Under the optimized conditions of pH = 2.2, C_o (2,4-D) = 40 ppm, and a catalyst-to-volume ratio of 0.5 g L^{-1}, the 3% AgNPs/g-C_3N_4 showed a weak propensity for 2,4-D adsorption, while almost complete oxidation and degradation of 2,4-D were observed after 210 minutes of illumination. The AgNPs/g-C_3N_4 composites display a good stability and maintain a high photocatalytic performance during five reaction cycles. That indicate AgNPs/g-C_3N_4 catalyst is stable for the photocatalytic 2,4-D degradation, which is significant for its practical applications.

Theoretical calculations on the interaction between 2,4-D and g-C_3N_4, Ag/g-C_3N_4 was also performed. The calculated results show that the adsorption of 2,4-D on Ag-modified g-C_3N_4 is significantly more effective compared to pristine g-C_3N_4.

Data availability

Data for this article are available upon request from the corresponding author.

Author contributions

Phung Thi Lan, Nguyen Hoang Hao and Le Minh Cam conceived of the study and designed the experiments. Nguyen Trung Hieu, Nguyen Thi Thu Ha, synthesized the materials. Nguyen Hoang Hao and C. Trevor Brown performed the material characterization and data analysis. Phung Thi Lan, C. Trevor Brown and Le Minh Cam wrote the manuscript. Nguyen Hoang Hao and Le Minh Cam supervised the project. All the authors contributed to the final version of the manuscript.

Conflicts of interest

The authors declare that they have no conflicts of interest.

Acknowledgements

This work is funded by the Ministry of Science and Technology in Vietnam under grant no. ĐTĐL.CN-66/19 and the Ministry of Education and Training under grant no. B2022-TDV-06.

References

1 J. Walters, Environmental fate of 2,3-dichlorophenoxyacetic acid, *Environ. Monit. Pest. Manage.*, 2021, **3510**, 1–18.
2 N. R. Zuanazzi, N. d C. Ghisi and E. C. Oliveira, Analysis of global trends and gaps for studies about 2,4-D herbicide toxicity: A scientometric review, *Chemosphere*, 2020, **241**, 125016.
3 H. K. Hue, L. V. Anh and D. B. Trong, Study of the adsorption of 2,4-dichlorophenoxyacetic acid from the aqueous solution onto activated carbon, *Vietnam J. Chem.*, 2018, **56**(2), 208–213.
4 J. Goscianska and A. Olejnik, Removal of 2,4-D herbicide from aqueous solution by amino silane grafted mesoporous carbons, *Adsorption*, 2019, **25**, 345–355.
5 S. F. A. Shattar, N. A. Zakaria and K. Y. Foo, Preparation of a montmorillonite-derived adsorbent for the practical treatment of ionic and nonionic pesticides, *J. Mater. Res. Technol.*, 2019, **8**(5), 4713–4724.
6 M. S. Fernando, A. A. D. S. Onélia and G. A. V. Melissa, Adsorption of herbicide 2,4-D from aqueous solution using organo-modified bentonite clay, *Environ. Sci. Pollut. Res.*, 2019, **26**(18), 18329–18342.
7 N. S. Trivedi and S. A. Mandavgane, Fundamentals of 2, 4 Dichlorophenoxyacetic Acid Removal from Aqueous Solutions, *Sep. Purif. Rev.*, 2018, **47**(4), 337–354.
8 X. Lü, Q. Zhang, W. Yang, X. Li, L. Zeng and L. Li, Catalytic ozonation of 2,4-dichlorophenoxyacetic acid over novel Fe–Ni/AC, *RSC Adv.*, 2015, **5**, 10537–10545.
9 J. L. Rodríguez, T. Poznyak, M. A. Valenzuela, H. Tiznado and I. Chairez, Surface interactions and mechanistic studies of 2,4-dichlorophenoxyacetic acid degradation by catalytic ozonation in presence of Ni/TiO_2, *Chem. Eng. J.*, 2013, **222**, 426–434.
10 G. C. González, C. Julcour, H. Chaumat, U. Jáuregui-Haza, H. Delmas and Henri, Degradation of 2,4-dichlorophenoxyacetic acid by photolysis and photo-Fenton oxidation, *J. Environ. Chem. Eng.*, 2018, **6**(1), 874–882.
11 W. Jiuqing, X. Jun, C. Xiaobo and X. Li, A review on gC_3N_4-based photocatalysts, *Appl. Surf. Sci.*, 2017, **391**, 72–123.
12 G. Dong, Y. Zhang, Q. Pan and J. Qiu, A fantastic graphitic carbon nitride (g-C_3N_4) material: Electronic structure, photocatalytic and photoelectronic properties, *J. Photochem. Photobiol., C*, 2014, **20**, 33–50.
13 L. Xibao, K. Bangbang, D. Fan, Z. Zhiqiang, L. Xudong, H. Lu, H. Juntong, F. Zhijun, C. Zhi, X. Jilin, P. Biaolin and L. W. Zhong, Enhanced photocatalytic degradation and H_2/H_2O_2 production performance of S-pCN/WO2.72 S-scheme heterojunction with appropriate surface oxygen vacancies, *Nano Energy*, 2021, **81**, 105671.
14 X. Li, T. Han, Y. Zhou, Y. Xie, Y. Luo, J. Huang, Z. Chen and F. Deng, Photoelectrocatalytic hydrogen evolution and synchronous degradation of organic pollutants by pg-C_3N_4/β-FeOOH S-scheme heterojunction, *Sci. China: Technol. Sci.*, 2024, **67**(4), 1238–1252, DOI: **10.1007/s11431-023-2604-x**.
15 W. Yong, L. Qiang, W. NgieHing, S. Jaka, H. Juntong, D. Guoliang, H. Xifeng and L. Xibao, Near-infrared (NIR) light responsiveness of CuS/S–C_3N_4 heterojunction photocatalyst with enhanced tetracycline degradation activity, *Ceram. Int.*, 2022, **48**(1S), 2454–2469.
16 L. Runlu, C. Zhixin, Y. Yao, L. Yao, A. C. Waqas, W. Dawei and Z. Shenmin, Recent advancements in g-C_3N_4-based photocatalysts for photocatalytic CO_2 reduction: a mini review, *RSC Adv.*, 2020, **10**, 29408.
17 Y. Hu, X. Li, W. Wang, F. Deng, L. Han, X. Gao, Z. Feng, Z. Chen, J. Huang, F. Zeng and F. Dong, Bi and S Co-doping g-C_3N_4 to Enhance Internal Electric Field for Robust Photocatalytic Degradation and H2 Production, *Chin. J. Struct. Chem.*, 2022, **41**(6), 2206069–2206078.
18 R. Liu, Y. Liu, C. Liu, S. Luo, Y. Teng, L. Yang, R. Yang and Q. Cai, Enhanced photoelectrocatalytic degradation of 2,4-dichlorophenoxyacetic acid by $CuInS_2$ nanoparticles deposition onto TiO_2 nanotube arrays, *J. Alloys Compd.*, 2011, **509**(5), 2434–2440.
19 Y. P. Zang, L. P. Li, X. G. Li, R. Lin and G. S. Li, Hybridization of brookite TiO_2 with g-C_3N_4: a visible-light-driven photocatalyst for As^{3+} oxidation, MO degradation and water splitting for hydrogen evolution, *J. Mater. Chem. A*, 2014, **2**, 15774–15780.
20 M. Hepel and J. Luo, Photoelectrochemical mineralization of textile diazo dye pollutants using nanocrystalline WO_3 electrodes, *Electrochim. Acta*, 2001, **47**(5), 729–740.
21 S. Patnaik, D. P. Sahoo and K. Parida, An overview on Ag modified g-C_3N_4 based nanostructured materials for energy and environmental applications, *Renewable Sustainable Energy Rev.*, 2018, **82**(1), 1297–1312.
22 S. Tonda, S. Kumar and V. Shanker, Surface plasmon resonance-induced photocatalysis by Au nanoparticles decorated mesoporous g-C_3N_4 nanosheets under direct sunlight irradiation, *Mater. Res. Bull.*, 2016, **75**, 51–58.
23 C. Han, L. Ge, C. Chen, Y. Li, Z. Zhao, X. Xiao and J. Zhang, Site-selected synthesis of novel Ag@AgCl nanoframes with

efficient visible light induced photocatalytic activity, *J. Mater. Chem. A*, 2014, **2**(31), 12594–12600.

24 R. F. Dong, B. Z. Tian, C. Y. Zeng, T. Y. Li, T. T. Wang and J. L. Zhong, Ecofriendly Synthesis and Photocatalytic Activity of Uniform Cubic Ag@AgCl Plasmonic Photocatalyst, *J. Phys. Chem. C*, 2013, **117**, 213–220.

25 X. Yao, X. Liu and X. Hu, Synthesis of the Ag/AgCl/g-C_3N_4 Composite with High Photocatalytic Activity under Visible Light Irradiation, *ChemCatChem*, 2014, **6**(12), 1–11, DOI: **10.1002/cctc.201402487**.

26 T. Zhou, Y. Xu, H. Xu, H. Wang, Z. Da, S. Huang, H. Ji and H. Li, In situ oxidation synthesis of visible-light-driven plasmonic photocatalyst Ag/AgCl/g-C_3N_4 and its activity, *Ceram. Int.*, 2014, **40**, 9293–9301.

27 S. Zhang, J. Li, X. Wang, Y. Huang, M. Zeng and J. Xu, In Situ Ion Exchange Synthesis of Strongly Coupled Ag @AgCl/g C_3N_4 Porous Nanosheets as Plasmonic Photocatalyst for Highly Efficient Visible-Light Photocatalysis, *ACS Appl. Mater. Interfaces*, 2014, **6**(24), 22116–22125.

28 S. Djokic, Synthesis and Antimicrobial Activity of Silver Citrate Complexes, *Bioinorg. Chem. Appl.*, 2018, 7, DOI: **10.1155/2008/436458**.

29 L. Oprica, M. Andries, L. Zaharescu, L. Popescu, D. Pricop, D. Creanga and M. Balasoiu, Citrate-Silver nanoparticles and their impact on some environmentally beneficial fungi, *Saudi J. Biol. Sci.*, 2020, **27**(12), 3365–3375.

30 R. L. Spina, D. Mehn, F. Fumagalli, M. Holland, F. Reniero, F. Rossi and D. Gilliland, Synthesis of Citrate-Stabilized Silver Nanoparticles Modified by Thermal and pH Preconditioned Tannic Acid, *Nanomaterials*, 2020, **10**(10), 2031.

31 M. U. Rashid, M. Khairul and M. E. Quayum, Synthesis of Silver Nanoparticles (Ag-NPs) and their uses for Quantitative Analysis of Vitamin C Tablets, *J. Appl. Polym. Sci.*, 2013, **118**, 312–319.

32 P. S. Yerragopu, S. Hiregoudar, U. Nidoni and K. T. Ramappa, Chemical Synthesis of Silver Nanoparticles Using Trisodium Citrate, Stability Study and Their Characterization, *Int. Res. J. Pure Appl. Chem.*, 2020, **21**(3), 37–50.

33 K. Shameli, Synthesis and characterization of polyethylene glycol mediated silver nanoparticles by the green method, *Int. J. Mol. Sci.*, 2012, **13**(6), 6639–6650.

34 K. Shameli, M. B. Ahmad, A. Zamanian, P. Sangpour, P. Shabanzadeh, Y. Abdollahi and M. Zargar, Mohsen, Green biosynthesis of silver nanoparticles using Curcuma longa tuber powder, *Int. J. Nanomed.*, 2012, **7**, 5603–5610.

35 S. Cao, J. Low, J. Yu and M. Jaroniec, Polymeric Photocatalysts Based on Graphitic Carbon Nitride, *J. Adv. Mater.*, 2015, **27**, 2150–2176.

36 T. Kashyap, S. Biswasi, A. R. Pal and C. Biswajit, Unraveling the Catalytic and Plasmonic Roles of g-C_3N_4 Supported Ag and Au Nanoparticles Under Selective Photoexcitation, *ACS Sustain. Chem. Eng.*, 2019, **7**(23), 19295–19302.

37 X. Bai, L. Wang, R. Zong and Y. Zhu, Photocatalytic activity enhanced via g-C_3N_4 nanoplates to nanorods, *J. Phys. Chem. C*, 2013, **117**, 9952.

38 L. Hao, J. Yue, M. Xinlong, L. Tongyao, Y. Linfeng, L. Bin, Y. Shu, W. Yongzhi and W. Yuhua, Construction of a well-dispersed Ag/graphene-like g-C_3N_4 photocatalyst and enhanced visible light photocatalytic activity, *RSC Adv.*, 2017, **7**, 8688.

39 G. Devipriya, K. S. Adit, Q. Mohammad, K. G. Animes and R. P. Nageswara, Silver grafted graphitic-carbon nitride ternary hetero-junction Ag/gC_3N_4(Urea)-gC_3N_4(Thiourea) with efficient charge transfer for enhanced visible-light photocatalytic green H_2 production, *Appl. Surf. Sci.*, 2021, **558**, 149900.

40 H. Ji, F. Chang, X. F. Hu, W. Qin and J. W. Shen, Photocatalytic degradation of 2,4,6-trichlorophenol over g-C_3N_4 under visible light irradiation, *Chem. Eng. J.*, 2013, **218**, 183–190.

41 A. Adak, I. Das, B. Mondal, S. Koner, P. Datta and L. Blaney, Degradation of 2,4-dichlorophenoxyacetic acid by UV 253.7 and UV-H_2O_2: Reaction kinetics and effects of interfering substances, *Emerging Contam.*, 2019, **5**, 53–60.

42 M. Aleksandrzak, K. Sielicki and E. Mijowska, Enhancement of photocatalytic hydrogen evolution with catalysts based on carbonized MOF-5 and g-C_3N_4, *RSC Adv.*, 2020, **10**(7), 4032–4039.

43 M. Roškarič, G. Žerjav, M. Finšgar, J. Zavašnik and A. Pintar, Influence of the calcination duration of g-C_3N_4/TiO_2 "veggie-toast-like" photocatalyst on the visible-light triggered photocatalytic oxidation of bisphenol A, *J. Alloys Compd.*, 2023, **947**, 169585.

44 R. Hao, G. Wang, H. Tang, L. Sun, C. Xu and D. Han, Template-free preparation of macro/mesoporous g-C_3N_4/TiO_2 heterojunction photocatalysts with enhanced visible light photocatalytic activity, *Appl. Catal., B*, 2016, **187**, 47–58.

45 P. T. Lan, N. H. Hao and L. M. Cam, Study on the synthesis and photocatalytic performance of modified TiO_2 supported by g-C3N4 in the degradation of 2,4-dichlorophenoxyacetic acid, *ChemistrySelect*, 2024, **9**(1 of 13), e202305026, DOI: **10.1002/slct.202305026**.

46 R. Liu, W. Yang, G. He, W. Zheng, M. Li, W. Tao and M. Tian, Ag-Modified g-C_3N_4 Prepared by a One-Step Calcination Method for Enhanced Catalytic Efficiency and Stability, *ACS Omega*, 2020, **5**, 19615–19624.

47 C. Lin, Y. Sudong, Q. Wensheng, Z. Qian, Z. Jie and Z. Peng, Supramolecular Self-Assembly of Nitrogen-Deficient Ag/g-C_3N_4 Nanofiber Films with Enhanced Charge Transfer Dynamics for Efficient Visible-Light Photocatalytic Activity, *ACS Appl. Mater. Interfaces*, 2021, **13**, 49993–50004.

48 H. Ji, F. Chang, X. Hu, W. Qin and J. Shen, Photocatalytic degradation of 2,4,6-trichlorophenol over g-C_3N_4 under visible light irradiation, *Chem. Eng. J.*, 2013, **218**, 183–190.

49 R. Liu, Y. Liu, C. Liu, S. Luo, Y. Teng, L. Yang, R. Yang and Q. Cai, Enhanced photoelectrocatalytic degradation of 2,4-dichlorophenoxyacetic acid by $CuInS_2$ nanoparticles deposition onto TiO_2 nanotube arrays, *J. Alloys Compd.*, 2011, **509**, 2434–2440.

50 N. T. T. Ha, P. T. Be, P. T. Lan, N. T. Mo, L. M. Cam and N. N. Ha, Whether planar or corrugated graphitic carbon nitride combined with titanium dioxide exhibits better

photocatalytic performance?, *RSC Adv.*, 2021, **11**, 16351–16358.

51 T. T. H. Nguyen, M. C. Le and N. N. Ha, Understanding the influence of single metal (Li, Mg, Al, Fe, Ag) doping on the electronic and optical properties of g-C_3N_4: a theoretical study, *Mol. Simul.*, 2021, **47**(1), 10–17.

52 B. Christoph, E. Sebastian and G. Stefan, GFN2-xTB—An Accurate and Broadly Parametrized Self-Consistent Tight-Binding Quantum Chemical Method with Multipole Electrostatics and Density-Dependent Dispersion Contributions, *J. Chem. Theory Comput.*, 2019, **15**(3), 1652–1671.

53 B. Cordero, V. Gómez, A. E. Platero-Prats, M. Revé, J. Echeverría, E. Cremades, F. Barragán and S. Alvarez, Covalent radii revisited, *Dalton Trans.*, 2008, 2832–2838.